Dual-Band Balanced Bandpass Filter Using Slotlines Loaded Patch Resonators With Independently Controllable Bandwidths

Gaoya Dong, Weimin Wang, Yongle Wu, *Senior Member, IEEE*, Weidan Li, Yuanan Liu, and Manos M. Tentzeris, *Fellow, IEEE*

***Abstract*— A novel dual-band balanced bandpass filter structure is constructed by utilizing patch resonators and meandered slotlines (MSLs). The center frequencies and passband bandwidths of two differential-mode (DM) passbands can be controlled independently. Specifically, the fractional bandwidth (FBW) in a lower band with the level of S_{11} better than 15 dB ranges from 2.9% to 19.1%, and the FBW in an upper band with the level of S_{11} better than 15 dB is from 2.0% to 13.9%. Furthermore, isolation resistors are added in the middle of the patch resonators to improve the common-mode (CM) suppression across the given frequency range. To verify the proposed filter concept, two dual-band balanced filters with different bandwidths are designed, fabricated, and measured.**

***Index Terms*— Bandpass filter (BPF), dual-band, independently controllable bandwidth, meandered slotlines (MSLs).**

I. Introduction

BALANCED circuits have attracted tremendous attention in recent years due to the high immunity to environmental noises, enhanced signal-to-noise ratio, low crosstalk, and low electromagnetic interference (EMI), compared with the single-end counterparts. With the rapid growth of multiband wireless communication systems, multiband balanced bandpass filters (BPFs) are proposed in [1]–[9]. Stub-loaded resonators (SLRs) [1] and [2], stepped-impedance resonators (SIRs) [3], [4], and coupled-line structures [5]–[8] are adopted to design multiband balanced BPFs. To further reduce the circuit size, composite right-/left-handed (CRLH) transmission lines (TLs) are employed to design dual-band balanced filter. Moreover, the differential-mode (DM) passband bandwidths of multi-band balanced BPFs presented in [2]–[6] can be controlled independently.

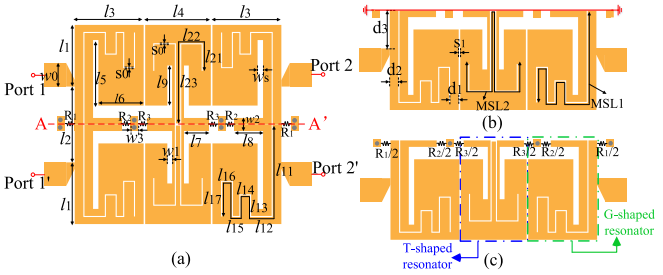

Fig. 1. (a) Layout of the designed dual-band balanced BPF. (b) Equivalent DM layout of the designed BPF. (c) Equivalent CM layout of the designed BPF.

In this letter, a compact dual-band balanced BPF structure is presented based on patch resonators and meandered slotlines (MSLs). The coupling coefficients and external factors of each DM passband can be independently adjusted by tuning the locations of MSLs and loading points as well as the coupling gaps, thus leading to independently controlled passband frequencies and bandwidths. The proposed dual-band balanced BPFs are all fabricated on the substrate with a thickness of 31 mil and a dielectric of 2.55 to verify the presented filter concept.

II. Operating Mechanism and Design Procedures

The designed dual-band balanced BPF schematic is shown in Fig. 1(a), which is symmetric about A–A′ plane. The symmetric plane A–A′ behaves as a perfect electric wall under DM excitation. Under common-mode (CM) excitation, the symmetric plane A–A′ acts as a perfect magnetic wall, which is conflicted with each other [10]. Thus, the CM signal cannot transmit, thus helping to realize high CM suppression. Moreover, the equivalent DM and CM layout is shown in Fig. 1(b) and (c), respectively.

Half-wavelength MSLs are etched on patch resonators to introduce resonance in the upper band. Define l_{x1} (l_{x2}) is the total length of MSL1 (MSL2). The electromagnetic (EM) fields produced by MSLs clearly inhabit both the substrate itself (ε_r) and the surrounding air (ε_0). Thus, the lengths of l_{x1} (l_{x2}) should be between $\lambda_g/2$ and $\lambda_0/2$, [11], [12]. As observed from the current intensity distribution exhibited in Fig. 2(a),

Manuscript received March 22, 2020; revised April 30, 2020; accepted May 17, 2020. Date of publication June 3, 2020; date of current version July 7, 2020. This work was supported in part by the Beijing Natural Science Foundation under Grant JQ19018, in part by the National Natural Science Foundations of China under Grant 61701041, Grant 61971052, and Grant 61821001, in part by the BUPT Excellent Ph.D. Students Foundation under Grant CX2019302, in part by the China Scholarship Council under Grant 201806470036, and in part by the Science and Technology Key Project of Guangdong Province, China under Grant 2019B010157001. *(Corresponding authors: Weimin Wang; Yongle Wu; Weidan Li.)*

Gaoya Dong, Weimin Wang, Yongle Wu, and Yuanan Liu are with the Beijing Key Laboratory of Work Safety Intelligent Monitoring, School of Electronic Engineering, Beijing University of Posts and Telecommunications, Beijing 100876, China (e-mail: wangwm@bupt.edu.cn; wuyongle138@gmail.com).

Weidan Li is with the Guangdong Communications & Networks Institute, Guangzhou 510670, China (e-mail: liwd@gdcni.cn).

Manos M. Tentzeris is with the School of Electrical Computer Engineering, Georgia Institute of Technology, Atlanta, GA 30332 USA (e-mail: etentze@ece.gatech.edu).

Color versions of one or more of the figures in this letter are available online at http://ieeexplore.ieee.org.

Digital Object Identifier 10.1109/LMWC.2020.2995963

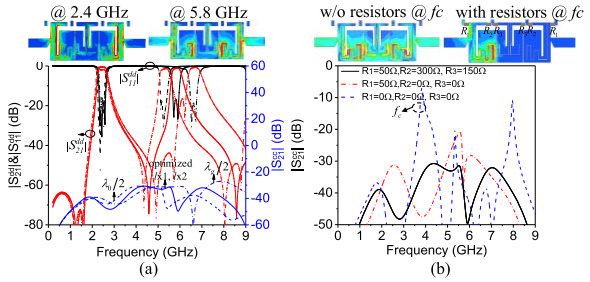

Fig. 2. (a) DM frequency responses with different values of l_{x1} and l_{x2}. (b) CM suppression of the presented BPF with different values of resistors.

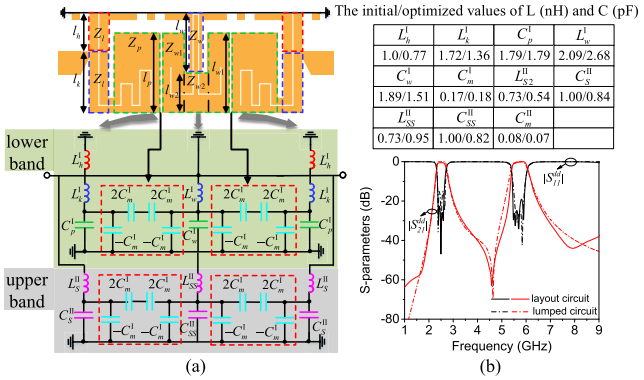

L_h^I	L_k^I	C_p^I	L_w^I
1.0/0.77	1.72/1.36	1.79/1.79	2.09/2.68
C_w^I	C_m^I	L_{S2}^{II}	C_S^{II}
1.89/1.51	0.17/0.18	0.73/0.54	1.00/0.84
L_{SS}^{II}	C_{SS}^{II}	C_m^{II}	
0.73/0.95	1.00/0.82	0.08/0.07	

Fig. 3. (a) Equivalent circuit for DM layout. (b) Frequency responses of the designed DM layout and equivalent circuit model.

the resonances in the lower band and the upper band are introduced by patch resonators and MSLs, respectively. According to Fig. 2(a), the upper band is centered at 6.55 and 5.33 GHz when l_{x1} and l_{x2} are chosen as $\lambda_g/2$ (18.8 mm) and $\lambda_0/2$ (25.6 mm) separately. Moreover, the center frequency in the upper band will shift to 5.86 GHz when the values of l_{x1} and l_{x2} are selected as 24.0 and 23.5 mm, respectively. The CM suppression performances with different isolation resistor values are plotted in Fig. 2(b). Accordingly, the CM suppression can be adjusted by tuning the values of R_1, R_2, and R_3.

According to [13], the required values of coupling coefficient ($M_{i,j}$) and external quality factor (Q_{ei}, Q_{eo}) can be calculated based on (1) to realize the three-order Chebyshev filtering response. The circuit elements of the low-pass prototype filter with S_{11} better than 15 dB are found to be $g_0 = 1$, $g_1 = 1.0316$, $g_2 = 1.1474$, $g_3 = 1.0316$, and $g_4 = 1.0$

$$M_{i,j} = \frac{\text{FBW}}{\sqrt{g_i g_{i+1}}} \quad (i \in 1, 2, \ldots, n), \quad Q_{ei} = Q_{eo} = \frac{g_0 g_1}{\text{FBW}}. \tag{1}$$

The upper passband and the lower passband are composed of the *LC* resonator. Thus, the equivalent *LC* circuit model can be adopted to analyze the operating mechanism in [14]–[18]. The equivalent circuit model of Fig. 1(b) is extracted as Fig. 3(a). Accordingly, the TLs in G- and T-shaped patch resonators can be modeled as inductors L_h^I, L_k^I, and L_w^I. The values of L_h^I, L_k^I, and L_w^I can be calculated based on (2), which has been explained in [13]. Based on [13, p. 113], the low-impedance patch can be modeled as a capacitor, and the TL (l_k) connecting the loading point and low-impedance patch also contributes some capacitance. Thus, the capacitor value (C_p^I) of G-shaped resonator can be deduced as (3). The low-impedance patch of T-shaped resonator can be seen

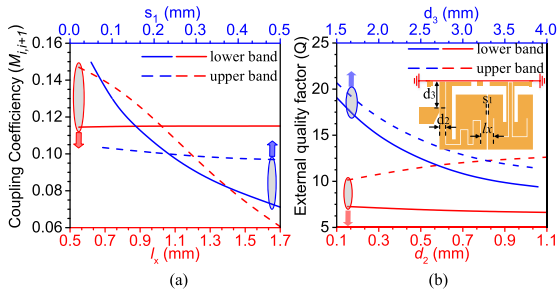

Fig. 4. (a) M^{I} and M^{II} with different values of l_x and s_1. (b) Q^{I} and Q^{II} with different values of d_2 and d_3.

as three rectangles. Thus, capacitor of T-shaped resonator can be considered as three paralleling capacitors, and the capacitor value (C_w^I) of T-shaped patch resonator can be derived as (4). The coupling introduced by adjacent resonators can be equivalent to the structure in the red dashed-line box, which is shown in Fig. 3(a). The coupling (C_m) can be deduced as (5), based on [13, p. 246]. The upper band introduced by MSLs can also be considered as *LC* resonators, and the values of inductor and capacitor in the upper band should satisfy (6). Assume the capacitor values (C_S^{II}, C_{SS}^{II}) all are 1 pF, the initial values of inductor (L_S^{II}, L_{SS}^{II}) can be obtained from (6). By employing the initial values calculated from (2) to (6), the parameters of the lumped-element circuit model are optimized to fit the EM simulation results, and the initial and optimized parameters values are listed in Fig. 3(b). The frequency responses of lumped circuit and EM simulation are depicted in Fig. 3(b), which shows good agreements

$$L_x^{\text{I}} = Z_x \tan(2\pi \cdot l_x/\lambda)/\omega, \quad x \in (h, l, w) \tag{2}$$

$$C_p^{\text{I}} = \frac{1}{Z_p \cdot \omega} \tan\left(\frac{2\pi \cdot l_p}{\lambda_{gp}}\right) + 2 \cdot \frac{1}{Z_l \cdot \omega} \tan\left(\frac{\pi l_k}{\lambda_{gL}}\right) \tag{3}$$

$$C_w^{\text{I}} = 2 \cdot \frac{1}{Z_{w1} \cdot \omega} \tan\left(\frac{2\pi \cdot l_{w1}}{\lambda_{gw1}}\right) + \frac{1}{Z_{w2} \cdot \omega} \tan\left(\frac{2\pi \cdot l_{w2}}{\lambda_{gw2}}\right) \tag{4}$$

$$C_m^{\text{I}} = M_{ij} \cdot \sqrt{C_p^{\text{I}} \cdot C_w^{\text{I}}} \tag{5}$$

$$f^{\text{II}} = 1/2\pi \sqrt{L_y^{\text{II}} \cdot C_y^{\text{II}}}, \quad y \in (s, ss). \tag{6}$$

The coupling coefficients between adjacent resonators with different parameter values are exhibited in Fig. 4(a). It can be seen from the blue lines in Fig. 4(a) that a reduced s_1 results in large M_{ij}^I and M_{ij}^{II}. The red lines in Fig. 4(a) indicates that M_{ij}^I can be adjusted by l_x, while M_{ij}^{II} cannot be affected by l_x. The external quality factors of G-shaped resonator in the lower band (Q_e^I) and upper band (Q_e^{II}) with different parameter values are shown in Fig. 4(b). Unfortunately, the conventional method cannot be adopted to simulate and calculate the values of Q_e^I and Q_e^{II} due to radiation introduced by MSLs. By constructing a two-order filter based on two symmetrical G-shaped patch resonators, Q_e^I and Q_e^{II} can be obtained from simulated fractional bandwidth (FBW) and (1). From blue lines shown in Fig. 4(b), a reduced d_3 results in large Q_e^I and Q_e^{II}. The red lines plotted in Fig. 4(b) indicate that Q_e^{II} can be adjusted by changing d_2, while M_{ij}^{II} almost remains constant with various d_2. Therefore, the external quality factors (Q_e^I, Q_e^{II}) and coupling coefficients (M_{ij}^I, M_{ij}^{II}) of two DM passbands can be controlled independently, thus resulting in controllable DM bandwidths.

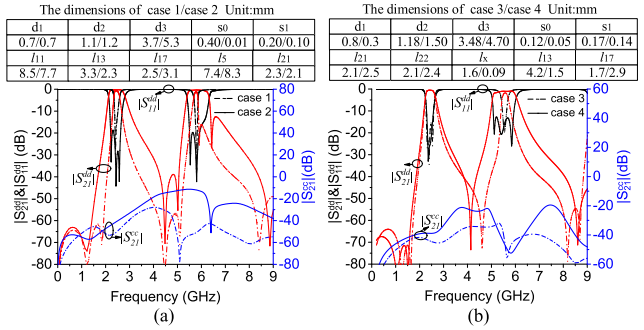

Fig. 5. (a) Frequency responses with different bandwidths in the lower band. (b) Frequency responses with different bandwidths in the upper band.

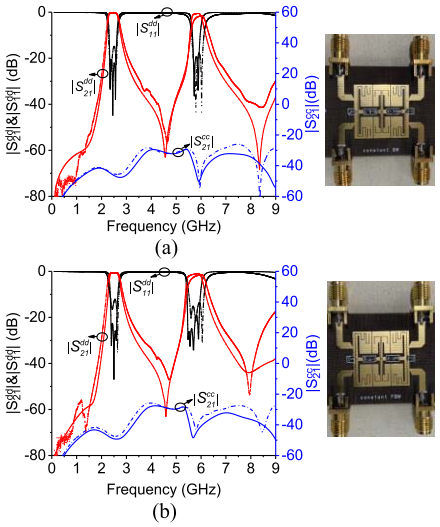

Fig. 6. (a) Simulated (solid lines) and measured (dashed lines) results of balanced (a) BPF1 and (b) BPF2. The specific parameters of BPF1 (BPF2), unit (mm): $w_0 = 2.2$ (2.2), $w_1 = 0.45$ (0.45), $w_2 = 1.2$ (1.2), $w_3 = 0.7$ (0.7), $l_1 = 5.4$ (5.7), $l_2 = 7.5$ (7.0), $l_3 = 6.4$ (6.4), $l_4 = 6.1$ (6.1), $l_5 = 6.0$ (6.0), $l_6 = 4.2$ (4.2), $l_7 = 2.2$ (2.2), $l_8 = 2.6$ (2.6), $l_9 = 3.9$ (3.7), $l_{11} = 8.5$ (8.5), $l_{12} = 2.0$ (2.0), $l_{13} = 3.1$ (2.0), $l_{14} = 1.0$ (1.0), $l_{15} = 0.7$ (0.7), $l_{16} = 1.0$ (1.0), $l_{17} = 2.4$ (3.2), $l_{21} = 2.0$ (3.4), $l_{22} = 2.0$ (2.0), $l_{23} = 7.4$ (7.4), $l_x = 1.6$ (1.8), $s_1 = 0.15$ (0.1), $s_0 = 0.1$ (0.1), $d_1 = 0.8$ (0.8), $d_2 = 0.8$ (1.25), and $d_3 = 3.9$ (4.2). Unit (Ω): $R_1 = 50$ (50), $R_2 = 300$ (350), and $R_3 = 150$ (200).

By employing the presented substrate above, the simulated frequency responses with the narrowest and widest DM passband bandwidths are shown in Fig. 5. Moreover, the detailed parameter values under different cases are also given in Fig. 5, and the other parameter values are the same as the parameter values in designed BPF1, which are given in Fig. 6. As observed in Fig. 5(a), the narrowest and widest passband bandwidths in the lower band are 2.9% and 19.1% with the level of S_{11} better than 15 dB. According to Fig. 5(b), in the upper band, the narrowest and widest passband bandwidths of S_{11} with the level better than 15 dB are 2.0% and 13.9%, while the passband bandwidth in the lower band almost remains constant.

Based on the above analysis, the detailed design procedures of the proposed dual-band BPF are summarized as follows.

1) Given the required center frequency (f^{I}, f^{II}), DM passband bandwidths, CM suppression level.
2) Calculate the required values of M_{ij}^{I}, Q_e^{I}, M_{ij}^{II}, and Q_e^{II} based on (1).
3) Design G- and T-shaped patch resonators etched with MSLs. The length of MSL1 (MSL2) should be between $\lambda_g/2$ and $\lambda_0.2$. Moreover, Q_e^{I} and Q_e^{II} can be adjusted by tuning the values of d_2 and d_3, based on Fig. 4(b).
4) Optimize return losses in two DM passbands by changing the values of l_x and s_1, based on Fig. 4(a).
5) Adjust the CM suppression performance by tuning the values of R_1, R_2, and R_3.
6) Return to step (3) until the simulated results meet the requirements given in step (1).

TABLE I

COMPARISONS WITH OTHER BALANCED DUAL-BAND BPFS

BPFs	CF (GHz)	IL (dB)	3-dB FBW (%)	CM level (dB)	Size	ICBW	Out-of-band Rejection (dB)
[2]	1.77/3.50	2.01/2.62	6.2/3.5	20	0.087	Y	1.20 f^{H}(>30 dB)
[3]	1.75/3.64	2.00/1.10	2.0/5.0	23	0.038	Y	2.16 f^{H}(>40 dB)
[4]	2.44/5.57	1.78/2.53	16.4/8.6	27	0.230	Y	/
Type I in [5]	2.40/3.51 5.20	2.43/3.50 3.60	9.0/5.5 4.0	32	0.245	Y	1.35 f^{H}(>10 dB)
Type II in [5]	1.54/2.45 3.58/5.2	1.9/2.8 3.7/4.6	11.0/4.9 8.8/5.0	32	0.245	Y	1.25f^{H}(>20 dB)
[9]	2.38/3.59	1.34/1.03	1.3/0.9	30	0.007	N	1.67 f^{H}(>27 dB)
BPF1	2.45/5.86	0.35/1.55	18.6/7.8	25.0	0.046	Y	1.58 f^{H}(>30 dB)
BPF2	2.51/5.81	0.51/1.42	19.6/10.9	26.5	0.046	Y	1.58 f^{H}(>20 dB)

f^{H}: is the center frequency of highest passband among the presented filter

III. SIMULATED AND MEASURED RESULTS

The photographs and detailed dimensions of the two fabricated dual-band balanced BPFs are given in Fig. 6. It can be observed from Fig. 6(a) that measured DM passbands in BPF1 are centered at 2.45 and 5.86 GHz, with a 3-dB FBW of 18.6% and 7.8% separately. In addition, the measured minimum insertion losses of the two DM passbands are 0.35 and 1.55 dB. For CM responses, the measured CM suppression is better than 44.8 dB for both operating passbands, and the CM suppression level is better than 25.0 dB ranging from dc to 9 GHz. As for BPF2, the two measured DM passbands are located at 2.51 and 5.81 GHz, with a 3-dB FBW of 19.6% and 10.9%, respectively. The measured minimum insertion losses of the two DM passbands are 0.51 and 1.42 dB. The measured CM suppression is better than 46.1 dB during operating passbands. From dc to 9 GHz, the measured CM suppression is better than 26.5 dB. The discrepancy between the measurement and simulation results in the upper band is due to the error of simulation as well as the error of MSL fabrication and measurement.

The comparisons of the proposed BPFs with other typical dual-band balanced BPFs are summarized in Table I. With regard to the comparisons, the presented approach has the advantages of wide passband bandwidth, low insertion loss, compact size, good out-of-band rejection, and independently controllable passband bandwidth (ICBW), which is suitable for engineering application.

IV. CONCLUSION

In this letter, a dual-band balanced BPF structure with controllable passband bandwidth is proposed based on patch resonators and MSLs, and isolation resistors are employed to obtain good CM suppression. The detailed design procedures are given, which is helpful for the application of dual-band balanced BPFs.

REFERENCES

[1] F. Wei *et al.*, "Compact balanced dual- and tri-band bandpass filters based on stub loaded resonators," *IEEE Microw. Wireless Compon. Lett.*, vol. 25, no. 8, pp. 76–78, Feb. 2015.

[2] S.-X. Zhang, Z.-H. Chen, Q.-X. Chu, and N. Shinohara, "Design of balanced dual-band bandpass filter with controllable bandwidths," in *Proc. Asia–Pacific Microw. Conf. (APMC)*, Dec. 2016, pp. 1–3.

[3] J. Tang, H. Liu, and Y. Yang, "Compact wide-stopband dual-band balanced filter using an electromagnetically coupled SIR pair with controllable transmission zeros and bandwidths," *IEEE Trans. Circuits Syst. II, Exp. Briefs*, Jan. 23, 2020, doi: 10.1109/TCSII.2020.2968922.

[4] J. Shi and Q. Xue, "Novel balanced dual-band bandpass filter using coupled stepped-impedance resonators," *IEEE Microw. Wireless Compon. Lett.*, vol. 20, no. 1, pp. 19–21, Jan. 2010.

[5] S.-X. Zhang, L.-L. Qiu, and Q.-X. Chu, "Multiband balanced filters with controllable bandwidths based on slotline coupling feed," *IEEE Microw. Wireless Compon. Lett.*, vol. 27, no. 11, pp. 974–976, Nov. 2017.

[6] Y.-H. Cho and S.-W. Yun, "Design of balanced dual-band bandpass filters using asymmetrical coupled lines," *IEEE Trans. Microw. Theory Techn.*, vol. 61, no. 8, pp. 2814–2820, Aug. 2013.

[7] F. Bagci, A. Fernandez-Prieto, A. Lujambio, J. Martel, J. Bernal, and F. Medina, "Compact balanced dual-band bandpass filter based on modified coupled-embedded resonators," *IEEE Microw. Wireless Compon. Lett.*, vol. 27, no. 1, pp. 31–33, Jan. 2017.

[8] L. Yang, W.-W. Choi, K.-W. Tam, and L. Zhu, "Balanced dual-band bandpass filter with multiple transmission zeros using doubly short-ended resonator coupled line," *IEEE Trans. Microw. Theory Techn.*, vol. 63, no. 7, pp. 2225–2232, Jul. 2015.

[9] Y. Song, H. W. Liu, W. Zhao, P. Wen, and Z. Wang, "Compact balanced dual-band bandpass filter with high common-mode suppression using planar via-free CRLH resonator," *IEEE Microw. Wireless Compon. Lett.*, vol. 28, no. 11, pp. 996–998, Nov. 2018.

[10] Y.-J. Lu, S.-Y. Chen, and P. Hsu, "A differential-mode wideband bandpass filter with enhanced common-mode suppression using slotline resonator," *IEEE Microw. Wireless Compon. Lett.*, vol. 22, no. 10, pp. 503–505, Oct. 2012.

[11] L.-P. Feng and L. Zhu, "Strip-loaded slotline resonator for compact differential-mode bandpass filters with improved upper stopband performance," *IEEE Microw. Wireless Compon. Lett.*, vol. 27, no. 2, pp. 108–110, Feb. 2017.

[12] T.-C. Edwards and M.-B. Steer, *Foundations for Microstrip Circuit Design*. Hoboken, NJ, USA: Wiley, 2016.

[13] J.-S. Hong and M.-J. Lancaster, *Microstrip Filter for RF/Microwave Application*. Hoboken, NJ, USA: Wiley, 2001.

[14] N. Intarawiset, S. Akatimagool, and S. Narongkul, "Analysis of microwave filter based on LC chips in microstrip circuitry using K-inverter approach," in *Proc. 6th Int. Conf. Tech. Edu. (ICTechEd6)*, Bangkok, Thailand, Mar. 2019, pp. 1–4.

[15] M. Xu, J. Tian, and P. Yang, "The design of LC resonator based bandpass filter embedded in LTCC substrate," in *Proc. 2nd Int. Conf. Power Electron. Intell. Transp. Syst. (PEITS)*, Shenzhen, China, Dec. 2009, pp. 301–305.

[16] C. Mao, Y. Zhu, Z. Li, and X. Ming, "Design of LC bandpass filters based on silicon-based IPD technology," in *Proc. 19th Int. Conf. Electron. Packag. Technol. (ICEPT)*, Shanghai, China, Aug. 2018, pp. 238–240.

[17] L. Huang, I. D. Robertson, and N. Yuan, "Substrate integrated waveguide bandpass filter with novel cascaded complementary electric-LC resonators," in *Proc. Eur. Microw. Conf.*, Nuremberg, Germany, Oct. 2013, pp. 33–36.

[18] J.-H. Chen and S. S. Liao, "Design of compact printed 2.4 GHz band-pass filter using LC resonator," in *Proc. Int. Conf. Adv. Mater. for Sci. Eng. (ICAMSE)*, Tainan, Taiwan, Nov. 2016, pp. 377–379.